

# Indentation Plastometry of Welds

Wenchen Gu, Jimmy Campbell, Yuanbo Tang, Hamed Safaie, Richard Johnston, Yuchen Gu, Cameron Pleydell-Pearce, Max Burley, James Dean, and Trevor William Clyne\*


This investigation concerns the application of the profilometry-based indentation plastometry (PIP) methodology to obtain stress–strain relationships for material in the vicinity of fusion welds. These are produced by The Welding Institute (TWI), using submerged arc welding to join pairs of thick steel plates. The width of the welds varies from about 5 mm at the bottom to about 40–50 mm at the top. For one weld, the properties of parent and weld metal are similar, while for the other, the weld metal is significantly harder than the parent. Both weldments are shown to be approximately isotropic in terms of mechanical response, while there is a small degree of anisotropy in the parent metal (with the through-thickness direction being slightly softer than the in-plane directions). The PIP procedure has a high sensitivity for detecting such anisotropy. It is also shown that there is excellent agreement between stress–strain curves obtained using PIP and via conventional uniaxial testing (tensile and compressive). Finally, the PIP methodology is used to explore properties in the transition regime between weld and parent, with a lateral resolution of the order of 1–2 mm. This reveals variations on a scale that would be very difficult to examine using conventional testing.

W. Gu, J. Campbell, M. Burley, J. Dean, T. W. Clyne  
Plastometrex Ltd.  
204 Science Park, Milton Road, Cambridge CB4 0GZ, UK  
E-mail: twc10@cam.ac.uk

Y. Tang  
Department of Materials  
University of Oxford  
Parks Road, Oxford OX3 3PH, UK

H. Safaie, R. Johnston, Y. Gu, C. Pleydell-Pearce  
Advanced Imaging of Materials  
Faculty of Science and Engineering  
Swansea University  
Fabian Way, Crymlyn Burrows, Skewen, Swansea SA1 8EN, UK

T. W. Clyne  
Department of Materials Science  
University of Cambridge  
27 Charles Babbage Road, Cambridge CB3 0FS, UK

 The ORCID identification number(s) for the author(s) of this article can be found under <https://doi.org/10.1002/adem.202101645>.

© 2022 The Authors. Advanced Engineering Materials published by Wiley-VCH GmbH. This is an open access article under the terms of the Creative Commons Attribution License, which permits use, distribution and reproduction in any medium, provided the original work is properly cited.

DOI: 10.1002/adem.202101645

## 1. Introduction

Profilometry-based indentation plastometry (PIP) is now starting to enter the mainstream of mechanical testing procedures. It is based on iterative finite element method (FEM) simulation of the indentation process, with the plasticity parameters (in a constitutive law) being repeatedly changed until an optimal agreement is reached between experimental and predicted outcomes. While the outcome used in much early work was the load–displacement plot, it has become clear that using the residual indent profile (i.e., the topography of the indent) offers major advantages. The superior reliability of PIP to the (instrumented indentation technique – (IIT)) methodology of converting a load–displacement plot to a stress–strain curve via analytic relationships has been clearly demonstrated.<sup>[1]</sup> Integrated facilities are now available that allow stress–strain curves to be inferred from a single indentation experiment

within a timescale of a couple of minutes or so. Recent papers cover in detail several relevant topics, including the effects of material anisotropy<sup>[2]</sup> and residual stresses,<sup>[3]</sup> and application of the methodology to very hard metals<sup>[4]</sup> and relatively thin layers.<sup>[5]</sup>

In general, the fidelity of PIP-derived stress–strain curves, when compared with those obtained via conventional tensile testing, is very good. A few caveats could be added to this statement. One is that the true stress–true plastic strain relationship must be one that can be well captured in an analytical expression (constitutive law). This can be done in most cases, although certain features, such as the load drop and initial burst of plastic strain associated with the escape of dislocations from “pinning” atmospheres of interstitial solute, cannot readily be captured. Certain other features, such as a “sigmoidal” shape associated with plasticity-induced phase transformations causing hardening, require novel constitutive laws.<sup>[6]</sup> Also, if a sample fractures “prematurely,” i.e., before it undergoes any necking and possibly before any yielding, then this point of failure cannot be captured. The methodology is not suitable for such highly brittle materials—at least if the focus is on failure.

It should also be noted that there is an underlying assumption (employed in virtually all FEM modeling of metal plasticity) that the true stress–true plastic strain relationship is between the von Mises (deviatoric) components of stress and strain, with the

hydrostatic components playing no role. As plastic deformation normally takes place with no volume change, this is generally expected to be valid (with the corollary that the same relationship will apply to both tensile and compressive testing). There are just a few cases in which this is invalid. Details are available in the literature.<sup>[7]</sup> Finally, there is sometimes what might look like a discrepancy in terms of the “sharpness” of the transition from elastic to fully plastic deformation. The mechanistic explanation for a relatively gradual transition is far from clear, although it has been noted<sup>[8,9]</sup> that it tends to be more pronounced with samples having a very fine grain size. In any event, small deviations in this regime are of very limited overall significance.

Advantages of the procedure, compared with conventional uniaxial testing, include minimal specimen preparation requirements and a capability to map properties over a surface on a relatively fine scale. These are also offered by hardness testing, but hardness numbers are not well-defined material properties, and they should be regarded as no better than semiquantitative guides to the plasticity of metals.<sup>[7]</sup> There are several types of samples for which the fine-scale mapping of material response, potentially including anisotropic effects, is a very attractive prospect. (Details of how anisotropy in the mechanical response of a sample can be detected via PIP are given in a previous publication.<sup>[2]</sup>) These certainly include the examination of variations in plastic response in the vicinity of welds and other types of joints. There is much interest in the local mechanical characteristics. This extends to exploring the probable susceptibility of a weld to the development of cracks and other defects, such as pores. This is certainly difficult to quantify using indentation, despite various claims (since discredited<sup>[10]</sup>) that it can be used to obtain fracture toughness parameters. However, reliable quantification of the plasticity characteristics is often a very useful guide to how cracking is likely to originate and develop. If the true stress–true strain characteristics of different regions of a weld (and surrounding parent metal) can be obtained, then FEM modeling of how the region will respond to various service loading conditions becomes possible, and this is likely to be very informative.

There have, in fact, been many indentation-based studies of welds. Unfortunately, most of them have been carried out on a very fine scale, such that the procedure could be described as “nanoindentation,” often involving sub-micron penetration and a deformed region with a lateral extent of no more than a few microns. A key finding from a detailed study over recent years<sup>[11]</sup> is the requirement to deform plastically a volume that is large enough for its mechanical response to be representative of the bulk, which usually requires it to be a “many-grained” assembly. This typically translates into a need for the indenter radius to be of the order of 0.5–1 mm, and the load capability to extend to the kilonewton range. This means that “nano-indenters” (typically having maximum loads of a few tens of Newtons at most) are completely unsuitable. While some studies based on such equipment appear to report consistent results, in practice, the scatter is always unacceptably high and in any event, deformation that is confined to a single grain virtually never reflects the bulk response of a polycrystal. A further conclusion, based on much practical experience,<sup>[11]</sup> is that a sphere is preferable to a “shaped” indenter, which commonly means one with sharp edges and apices. These create several practical and theoretical difficulties.

There have, however, been previous studies of welds involving spherical indentation on a suitably coarse scale. A number of these have been based on the so-called Automated Ball Indentation (ABI) system. This has been available for some time, largely based on publications<sup>[12,13]</sup> from the 1990s, and equipment has been marketed since that period by firms such as Frontics. The methodology is not entirely transparent from a scientific point of view, but in practical terms, it comprises the application of a progressively increasing load via a hard sphere (usually a cermet ball with a radius between about 0.3 and 0.8 mm), with periodic partial unloading. The penetration at the start of each unloading (“total depth”), and that obtained by extrapolating the unloading line back to zero load (“plastic depth”), are measured, with perhaps a dozen or so such operations being carried out altogether. Average values of the true stress and true strain associated with each unloading are obtained, using simple empirical equations. These involve the measured depths (and some arbitrarily adjustable parameters). Some simple manipulation of these data then allows the plasticity characteristics (commonly in the form of yield stress and ultimate tensile strength (UTS)) to be inferred. The underlying ideas on which these equations and procedures are based date back to David Tabor’s work<sup>[14]</sup> in the 1950s. They are sometimes referred to collectively under the heading of instrumented indentation technique (IIT)<sup>[1]</sup> and procedures of this type have frequently been implemented using nanoindenters. The loads used in the ABI methodology depend on indenter radius and the material being tested, but the ratio of final penetration depth to ball radius is often relatively high (greater than unity in some cases) and this commonly leads to required loads being in the kilonewton range.

The procedure certainly satisfies the requirements with respect to deforming a representative volume and inducing suitably high levels of plastic strain. The reliability and robustness of the analytical manipulations (involved in IIT) are, however, clearly open to question. A recent round-robin trial,<sup>[15]</sup> oriented toward components in the nuclear industry, involved six laboratories applying nominally the same ABI procedure to two different steels and one Zr alloy, after various heat treatments. It resulted in quite large variations (well over 20% in some cases) between the six sets of results, and agreement with the corresponding tensile test outcomes was also relatively poor. The actual conclusions of the trial were reasonably positive about the technique, although of course, this was an operation in which the participants had prior knowledge of the “correct” properties and also had some freedom to select certain parameter values. It was certainly felt that the standard ABI procedure is not sufficiently well developed for the required purposes in the nuclear industry.

In that case, the samples being tested were from large diameter pipes, which were expected to be fairly homogeneous. It was acknowledged that they could have exhibited anisotropy, although this was not explored experimentally. This is certainly a potential source of error, as indentation responses tend to be direction-averaged and the ABI procedure does not allow anisotropy to be detected. Furthermore, the issue of point-to-point variations in properties, which is clearly important for welds, did not arise in those trials. Comparisons with data from uniaxial testing clearly become more complex with welds. Several recent

studies<sup>[16–19]</sup> have involved the application of the ABI procedure to welds. Other spherical indentation work on welds has involved indenter radii from 50  $\mu\text{m}$ <sup>[20]</sup> up to over 1 mm.<sup>[21]</sup> These studies all involved some variant of the IIT approach. They were certainly all able to detect differences between weldment and parent metal properties and to study the transition between them, but without clear evidence that the inferred stress–strain curves were accurate and without, at least in most cases, being noticeably more informative than hardness testing profiles.

There have, however, been very few studies of welds using spherical indentation in combination with inverse FEM modeling. A number of authors<sup>[22–24]</sup> have used inverse FEM, but only in conjunction with fine scale and/or nonspherical indenter shapes, and focusing exclusively on the load–displacement plot as the target outcome. Various sensitivities would certainly have been inhibiting the extraction of reliable stress–strain curves, although some authors do claim consistent results. The current study is thus apparently the first PIP-based measurement of mechanical properties within and around fusion welds.

## 2. Experimental Procedures

### 2.1. Materials and Welding Conditions

Two submerged arc welds were created at The Welding Institute (TWI), both joining a pair of wide and long plates of low alloy steel (EN 10 025-2 (S355 J2 + N)), of thickness 25 mm. The compositional spec of this steel is shown in **Table 1**. The two welds involved the use of different (steel) filler metals, and their compositions (typically measured, post-welding) are also shown in **Table 1**. The specs of these three metals usually include approximate (minimum) values for yield stress and UTS: these values are given in **Table 2**. The higher alloying element levels (notably Ni and Mo) in the E111T1-K3M filler (Weld 2), compared with EM12K (Weld 1), confer appreciably higher strength. Such filler metal would, in practice, commonly be used to join correspondingly stronger parent plates, but for the purpose of this investigation, there was interest in exploring a system in which the weld exhibited markedly different properties from the parent.

The welding geometry is illustrated in **Figure 1**. Weld 1 involved 19 passes, while there were 17 for Weld 2. In both cases, the first two passes were carried out using the Metal Active Gas (MAG) process, in spray mode, with the arc being struck between the parent and the wire electrode, relatively low voltage and current being used, with gas shielding and no slag coverage. Subsequent passes used the conventional submerged arc welding (SAW) process, with a feed of granular flux creating a slag to cover the arc and the process being under somewhat closer

**Table 2.** Strength specs of the parent metal and the two filler metals.

Designation	Yield stress $\sigma_Y$ [MPa]	UTS $\sigma_{UTS}$ [MPa]
S355 J2 + N (Parent)	355	470–630
EM12K (Weld 1)	400	480–660
E111T1-K3M (Weld 2)	680	760–900

control, with no danger of weld spatter, etc. The operating parameters for both welds are shown in **Table 3**.

One of the main factors affecting the microstructure of a weld is the rate of heat input,  $Q$ , expressed as a quantity of heat energy injected per unit length of the weld (for a given weld sectional geometry). In the specification of EN 1011-1, the value of  $Q$  (in  $\text{kJ mm}^{-1}$ ) is given by

$$Q = \frac{kVI}{U} 10^{-3} \quad (1)$$

in which  $V$  is the arc voltage (V),  $I$  is the welding current (A),  $U$  is the travel speed ( $\text{mm min}^{-1}$ ), and  $k$  is a thermal efficiency factor that is dependent on the type of weld—having a value of 1.0 for SAW and 0.8 for MAG. Values of  $Q$  for each pass are shown in **Table 3**. One point to note here is that the heat input is quite accurately constant during each SAW pass. The overall cooling rate is also affected by the preheat temperature, but this is also fairly uniform throughout, so average cooling rates are likely to have been constant. Of course, local cooling rates are also affected by location within the weld, being higher for regions closer to the parent.

### 2.2. Sample Preparation

Relatively small sections were cut from the welded pairs of plates, incorporating short lengths of the welds (see **Figure 2**). These were taken from regions that were not close to the ends (run-on and run-off) of the plates, so they incorporated material produced under steady-state conditions. The three principal directions (axial, transverse, and through-thickness) are indicated in the figure, and the acronyms shown are used here when referring to particular planes and directions.

### 2.3. Microstructural Examination

Orthogonal and parallel (TT-TD/TD-AD/TT-AD) sections of the welded samples were metallographically prepared via standard grinding and polishing techniques. Care was taken to ensure that samples were free from residual strains introduced through the

**Table 1.** Compositional specs of the parent metal and the two filler metals.

Designation	Composition [wt%]													
	C	Mn	Si	P	S	Cu	Ni	Cr	Mo	Al	V	Nb	Ti	N
S355 J2 + N (Parent)	0.16	1.49	0.25	0.011	0.002	0.04	0.02	0.02	0.005	0.03	0.005	0.021	0.005	0.005
EM12K (Weld 1)	0.09	1.12	0.20	0.012	0.008	0.065	–	–	–	–	–	–	–	–
E111T1-K3M (Weld 2)	0.07	2.03	0.38	0.01	0.01	–	1.99	0.09	0.38	–	0.02	–	–	–

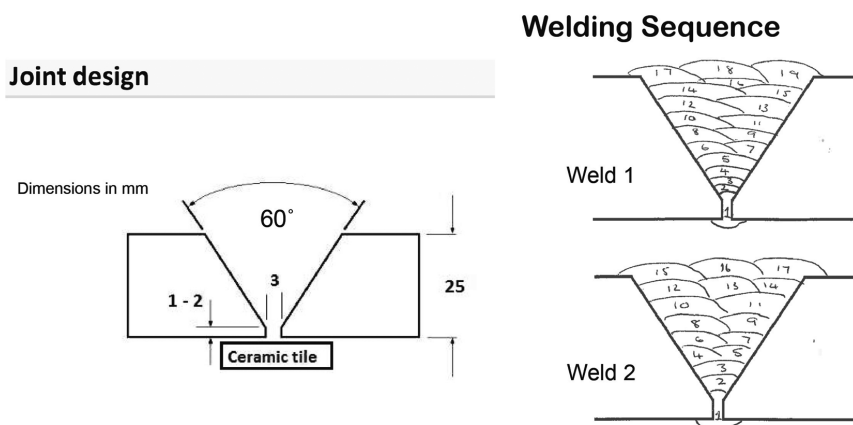


Figure 1. Welding geometry and dimensions.

Table 3. Operating parameters for production of the two welds.

Pass	Weld 1					Weld 2				
	$T$ [°C]	$I$ [A]	$V$ [V]	$U$ [mm min <sup>-1</sup> ]	$Q$ [kJ mm <sup>-1</sup> ]	$T$ [°C]	$I$ [A]	$V$ [V]	$U$ [mm min <sup>-1</sup> ]	$Q$ [kJ mm <sup>-1</sup> ]
1	15	176	24	300	0.68	50	240	24	300	0.92
2	15	227	25	300	0.91		280	27	500	1.21
3		500	28	550	1.53		500	28	500	1.68
4	75	550	28	500	1.85		550	30	550	1.80
5		550	30	500	1.98	95	550	30	550	1.80
6		550	30	500	1.98		550	30	550	1.80
7		550	30	550	1.80		550	30	550	1.80
8		550	30	550	1.80		550	30	550	1.80
9		550	30	550	1.80	150	550	30	550	1.80
10		550	30	550	1.80		550	30	550	1.80
11	170	550	30	550	1.80		550	30	550	1.80
12		550	30	550	1.80		550	30	550	1.80
13		550	30	550	1.80	190	550	30	550	1.80
14		550	30	550	1.80	65	550	30	550	1.80
15	140	550	30	550	1.80		550	30	555	1.78
16		550	30	550	1.80		550	30	500	1.98
17		550	30	550	1.80	135	550	30	500	1.98
18	195	550	30	550	1.80	–	–	–	–	–
19		550	30	550	1.80	–	–	–	–	–

grinding process. Finally, the material was polished using a sub-micron slurry OP-S. Microtexture determination was achieved through electron backscatter diffraction (EBSD). High spatial resolution data were acquired using a JEOL 7800F field emission scanning electron microscope, fitted with an Oxford Instruments Nordlys Max2 EBSD detector. This was calibrated using a cleaved silicon wafer of known crystallographic orientation (to within  $\pm 0.5^\circ$ ). Combined with stage and mounting tolerances, this gave an absolute angular accuracy of  $\approx 2^\circ$ . Larger area maps were acquired on a Carl Zeiss Evo LS, with an LaB<sub>6</sub> electron source fitted with an Oxford Instruments Swift Detector. This system has comparable angular accuracy and precision errors.

All maps were acquired with an accelerating voltage of 20 kV and a probe current of 14 nA. A step size of 0.2  $\mu\text{m}$  was applied to all maps. This was selected to provide sufficient spatial resolution to reveal the microtextural features of interest. The data were presented in the form of IPF<sub>x</sub> (for microtexture) and orientation distribution functions (for macrotexture).

## 2.4. Uniaxial Testing

Two types of tensile testing were carried out. The first involved using an Instron 3369, with a 50 kN capacity. Samples were rectangular in section, with the reduced section part having a width

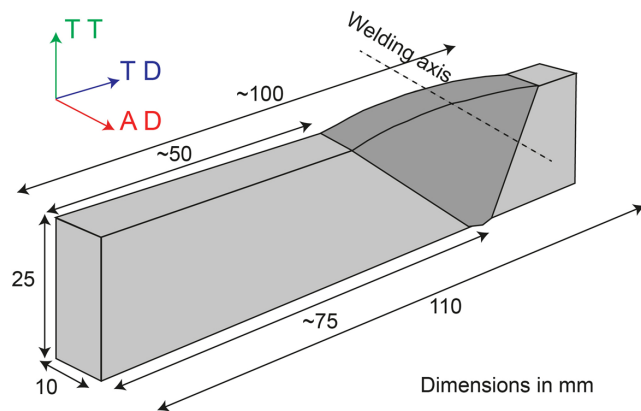


**Figure 2.** Geometry and dimensions of small sections cut from the large welded plates.

of 6 mm, a thickness of 4 mm, and a length of 30 mm, and the clip gauge itself being 25 mm long. The other type was carried out using an Instron electro-thermal mechanical testing system, with a 5 kN load cell. Samples were cut to a dog-bone shape, using electro discharge machining, to give flat (1 mm thick) samples with a gauge length of 7 mm and a gauge length width of 2 mm. This relatively compact geometry was designed particularly for testing the parent metal in the through-thickness direction (in which the total length was 25 mm). The strain was measured using a video extensometer, with an iMetrum system. Speckle patterns were applied on the surfaces to facilitate tracking. The focus was on the separation of speckles at both ends of the gauge length, i.e., the (nominal) strain was being measured in the same way as with a clip gauge. All samples were tested to fracture.

Compression tests were also carried out using an Instron 3369 loading frame. Samples were in the form of cylinders (4 mm diameter and 4 mm long). No lubricant was used. Displacement was measured using a Linear Variable Displacement Transducer, attached to the upper platen and actuated against the lower one. The nominal stress–strain curves presented here were corrected for “bedding-down” effects by extrapolation of the linear portion back to zero stress, giving the zero strain level.

The approach adopted for comparing results from uniaxial and indentation-based testing was first to use the PIP procedure to infer the true stress–true strain curve (as a set of parameter values in the Voce constitutive law) (see Section 2.5). These parameter values were then used to simulate both the tensile test and the compression test (with a specified friction coefficient). This led to nominal stress–nominal strain curves, which could be compared with the corresponding experimental plots. The value used for the friction coefficient was obtained by comparing<sup>[4]</sup> measured and modeled barrelling profiles along the length of the sample after the test.

## 2.5. Indentation Plastometry

The PIP setup used in this work is based on the geometry shown schematically in **Figure 3**. Four steps are involved in obtaining a tensile (or compressive) nominal stress–strain curve from a PIP test. These are as follows: (a) pushing a hard indenter into the sample with a known force, (b) measuring the (radially

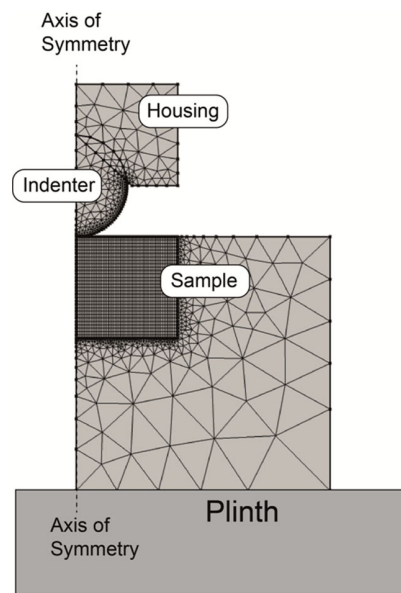


**Figure 3.** FEM mesh employed for PIP indentation.

symmetric) profile of the indent, (c) iterative FEM simulation of the test until the best-fit set of (Voce) plasticity parameter values is obtained, and (d) using the resultant (true) stress–strain relationship in FEM simulation of the tensile or compression test (with a friction coefficient required for the latter). The ball used was a WC-Co cermet with a radius of 1 mm. The loading took place over a period of about 30 s. The indent topographies were characterized with a stylus profilometer having a resolution of about 1  $\mu\text{m}$ . The indents typically had a width of about 1 mm.

## 3. Mechanical Characteristics

### 3.1. Parent Metal

Among the key areas of interest is the detection and characterization of any anisotropy or inhomogeneity, particularly within and around the weld, but also in the parent metal itself. In fact, as the welds were created under commercial conditions, which are in general aimed at minimizing both types of effects, neither was very pronounced. Nevertheless, careful study of them is important. **Figure 4** shows the outcome of PIP testing on both AD-TD (in-plane) and TT-TD (transverse) surfaces, with the geometry of these tests illustrated in the schematic diagram.

Three points can immediately be seen. One is that there is no in-plane anisotropy, as the profiles in different directions are identical (**Figure 4b**), i.e., the indents are radially symmetric. The second is that (**Figure 4c,d**) there is some anisotropy in the transverse plane, with material deforming more readily (creating higher pileups) in the TT (through-thickness) direction than in in-plane directions (TD or AD). The third is that there is little or no inhomogeneity in the through-thickness direction, as the profiles close to the free surfaces (“top” and “bottom”) are virtually identical to those in the center. (Of course, in large plates such as these, there is no expectation of inhomogeneity with changing in-plane location.)



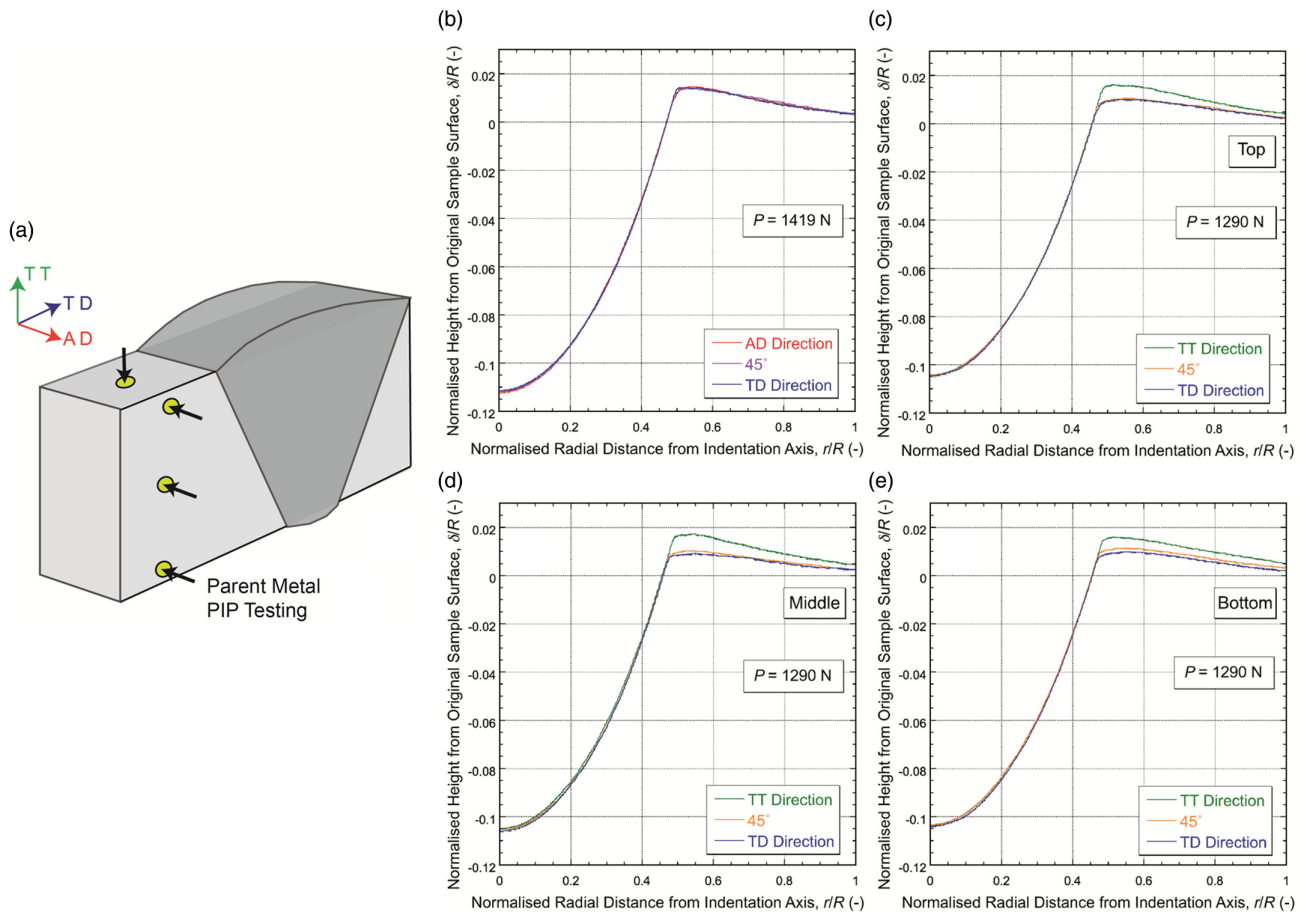


**Figure 4.** PIP testing of the parent metal, showing a) a schematic of the test geometry, b) measured indent profile from the top surface (AD-TD plane), and c–e) profiles at different depths in the transverse (TD-TT) plane.

Uniaxial testing, both tensile and compressive, was also carried out on the parent metal, in both in-plane and through-thickness directions. The in-plane testing was in both cases carried out in the TD direction. Comparison between PIP and uniaxial test outcomes was in both cases made by converting the PIP outcome (set of Voce parameter values) to a nominal stress–strain curve: this is valid only up to the onset of necking for the tensile testing (although the post-necking behavior can be obtained via FEM simulation of the test, using the specific dimensions of the test piece). The resulting plots are shown in **Figure 5**. Several points can again be noted. First, the uniaxial testing does pick up some initial “strain bursting,” although it is certainly not very pronounced. This effect is unsurprising in a steel with this composition: it is presumably associated with unpinning of dislocation arrays from their carbon “atmospheres.” This cannot be picked up via PIP testing (using a constitutive law, such as Voce, that cannot capture such an effect). However, the overall behavior is still being captured well via PIP, for both compression and tension. Second, the anisotropy picked up via PIP (**Figure 4c–e**) is detected by the tensile testing, although not by the compressive testing. Furthermore, the tensile testing shows that, while there is a clear difference, it is apparent only in the higher strain parts of the curve (close

to the onset of necking). The sense of the change is picked up correctly, with the through-thickness direction being a little “softer” than the in-plane directions. Furthermore, these observations are consistent with the fact that the anisotropy detected via asymmetry in the PIP indent is sensitive to the response at relatively high strains (being generated in the pileup). It is clear that PIP testing is a sensitive (and very convenient) method of detecting anisotropy, although it is also evident that the test will need to be modeled in a more comprehensive manner if its full characteristics are to be quantitatively captured.

### 3.2. Weldments

The profiles obtained by indenting into the TT-TD plane are shown in **Figure 6**, for both Welds, at three different depths below the free surface. (In fact, the results presented are from indents on the stub ends of tensile samples, although it was confirmed that indents in the orientations shown, i.e., into the TT-TD plane, gave the same results, which is consistent with the welds being isotropic.) Again, several features are apparent. First, there does not appear to be much variation with depth. Second, in contrast to the parent metal, there is little or no anisotropy apparent in these profiles. This was also the case for indents

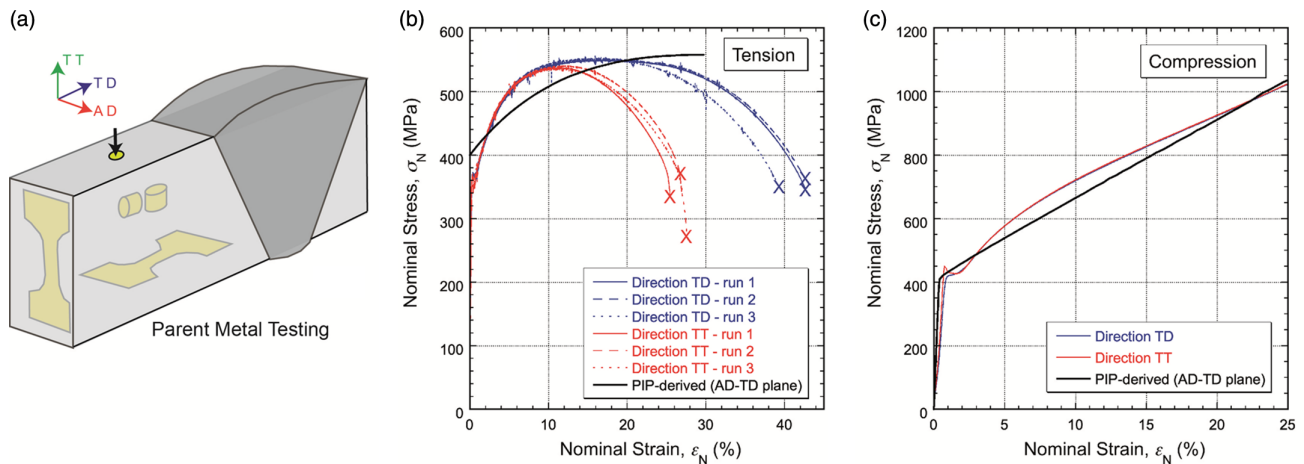


**Figure 5.** Comparison between PIP-derived and directly measured uniaxial test outcomes for the parent metal, showing a) a schematic of the test geometry, b) nominal stress–strain plots in tension, and c) nominal stress–strain plots in compression.

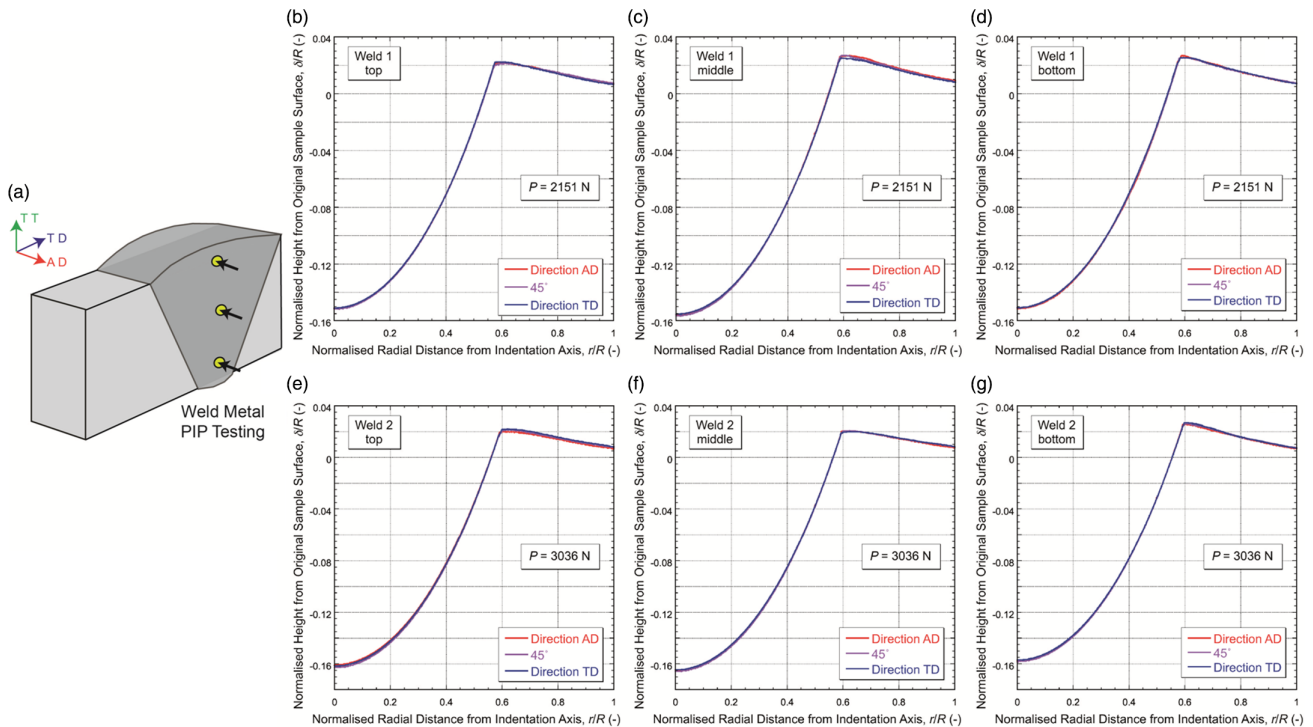


**Figure 6.** PIP testing of the two weld metals, showing a) a schematic of the test geometry, b–d) measured indent profiles (AD-TD plane) at different locations for Weld 1, and e–g) corresponding data for Weld 2.

in the AD-TD plane, so the weldments are approximately isotropic, as well as fairly homogeneous—although there are naturally some variations in properties with the location in the vicinity of the boundary with the parent metal (see Section 3.3).

A comparison is shown in **Figure 7** between PIP-derived and directly-measured tensile stress–strain curves. The latter also indicates that, for both welds, there is little variation in properties with the location. In general, the agreement between PIP and direct curves is good. Weld 1 has similar properties to those of the parent, having slightly higher yield stress, but a lower

work hardening rate, such that the UTS is similar (at about 550–600 MPa). In contrast, as planned, the hardness of Weld 2 is appreciably higher than that of the parent, with a yield stress of around 700 MPa and a UTS of about 800 MPa.

### 3.3. Transition Regime

A summary is shown in **Figure 8** of the outcome of a series of PIP tests on the TD-AD plane, in the vicinity of the fusion boundary. Yield stress and UTS values are plotted as a function of distance

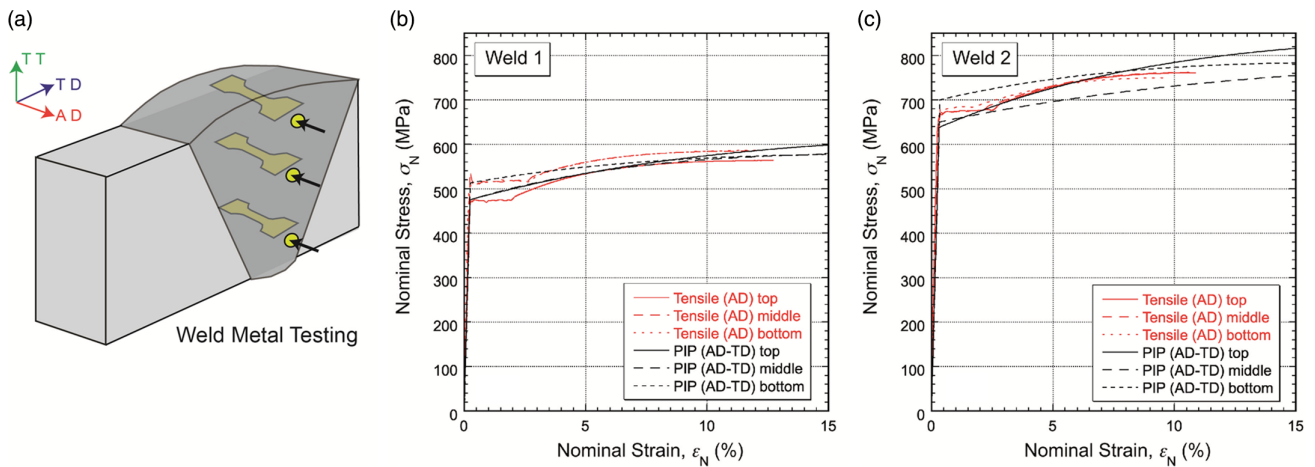


**Figure 7.** Comparison between PIP-derived and directly measured tensile test outcomes for the welds, showing a) a schematic of the test geometry, b) nominal stress–strain plots for Weld 1, and c) corresponding data for Weld 2.

from the weld centerline, for both welds. Of course, no comparison can be made with corresponding uniaxial test outcomes, due to their poor spatial resolution, although the results are certainly consistent with those test outcomes in regions remote from the boundary. For example, it can be seen in Figure 5b that the yield stress (YS) of the parent metal is about 350–400 MPa, while the UTS is about 550 MPa. Similarly, Figure 7 shows that, for Weld 1, the corresponding values are about 500 and 600 MPa, while for Weld 2, they are about 700 and 750–800 MPa. These values are close to those in Figure 8 for regions not close to the boundary.

In both cases, and for both parent and weld, there are indications that the regions close to the boundary (i.e., within about 5 mm) are slightly harder, relative to the same constituent further away. It may be that the higher cooling rate experienced by the weld close to the parent leads to a slightly finer microstructure, which is somewhat harder. Similarly, the parent metal close to the weld (in a “heat affected zone”) will have undergone a heat treatment that could have made it slightly harder. The changes in

parent properties are certainly very similar in the two cases, which is consistent with those regions having experienced very similar thermal histories. These comments are, however, offered in a general vein, and no attempt is made here to test any of the suggestions further—for example, by specifically subjecting the parent to heat treatments, or by careful study of local microstructures. Nevertheless, it does seem clear that PIP measurements have a useful capability for property mapping on this kind of scale.

### 3.4. Correlation with Microstructure

The microstructural objectives are limited to examining the grain structure and texture of parent and weld metals (remote from the boundary regions) and checking on consistency with the mechanical testing data. Of course, even this is not so simple, as 3D characterization of texture is always relatively complex. As it happens, the mechanical property results suggest that both

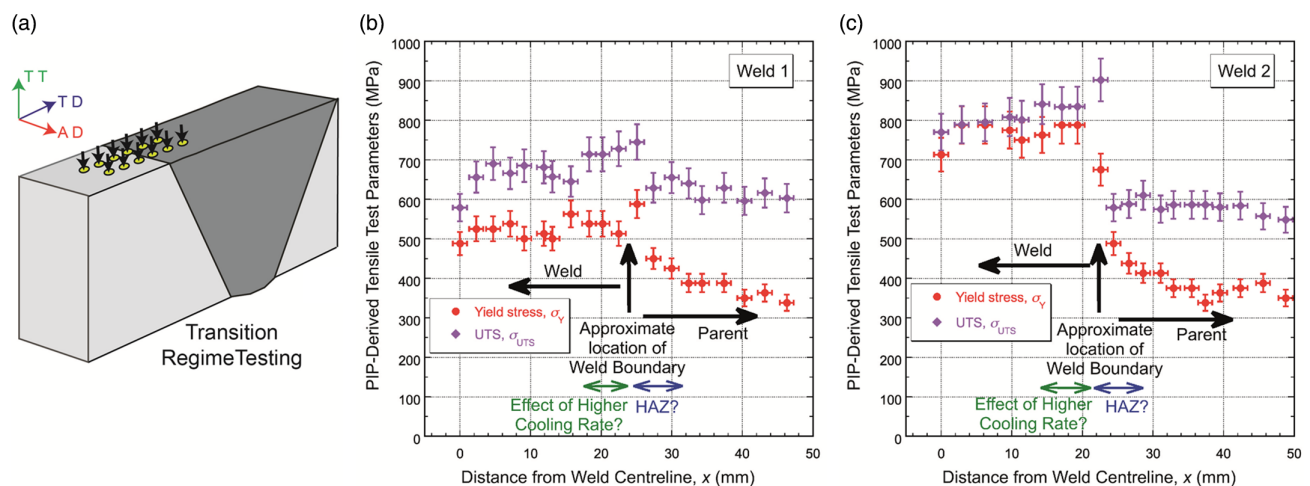


**Figure 8.** PIP-derived outcomes for the parent–weld transition regions, showing a) a schematic of the test geometry, b) a plot of tensile yield stress and UTS against location for Weld 1, and c) equivalent data for Weld 2.



weldments are isotropic, and hence probably untextured, while the parent has in-plane isotropy and only very weak anisotropy in transverse sections. The EBSD data are at least broadly consistent with these results. For example, **Figure 9** presents information for the parent metal. The grain structure is relatively coarse, with an average size of about  $30\ \mu\text{m}$ . In the in-plane section (**Figure 9a**), grains are approximately equiaxed, which is consistent with in-plane isotropy. The corresponding pole figure also shows no clear texture. (There are a couple of relatively high  $\chi$ -random contours, but there is nothing systematic and such features are almost certainly due to counting statistics.) The transverse section (**Figure 9b**) confirms that there is some grain shape anisotropy, with the grains somewhat thinner in the through-thickness direction. This is probably inherited from rolling operations. This could be consistent with the observed slight anisotropy in mechanical properties, although there is again no evidence in the pole figure of systematic texture.

Corresponding information for the welds is shown in **Figure 10**. One clear feature is that the grain structures are finer than for the parent. However, the relatively large ( $\approx 100\ \mu\text{m}$ ) regions exhibiting consistent orientations (preferential color bias) are probably prior austenite grains—although the original

solidification would have been of the delta-ferrite phase. The ferrite grains in the final microstructure will tend to exhibit an orientation relationship (Kurdjumov–Sachs or Nishiyama–Wasserman) with the parent austenite, giving rise to the observed effects. This makes it a little more difficult to obtain representative texture data, as a relatively large number of these prior austenite grains should ideally be incorporated in the analysis. Nevertheless, the pole figures shown here do indicate that there is little or no clear texture in these structures (accepting that the odd high contour, with no systematic distribution, does not reflect genuine texture). Moreover, for both welds, the grain structures look very similar in the two sections (unlike the parent). These observations are all consistent with the idea that the weldments are isotropic. This is a commercial objective when optimizing the welding conditions.

## 4. Conclusions

Two submerged arc welds (supplied by TWI), each joining a pair of large steel plates of thickness 25 mm, have been mechanically tested, using both conventional uniaxial (tensile and compressive) loading and the novel procedure of PIP. The fundamental outcome of a PIP test is the relationship between the true von Mises stress and the true plastic von Mises strain. This can be used (via FEM modeling) to predict outcomes for virtually any type of plasticity test, including the nominal stress–nominal strain curves obtained during tensile and compressive testing.

The testing has encompassed both the parent metal (the same for both welds) and the weld metal (different in the two cases, with one having a similar hardness to the parent and the other being considerably harder). It has covered the basic plasticity characteristics, plus a check for possible anisotropy and inhomogeneity in both constituents. In addition, the transition regime between weld and parent has been explored, using only the PIP test, which has a far superior spatial resolution to the uniaxial tests.

It is shown that there is a high degree of consistency between results obtained from these three types of tests. Both the weld metals and the parent are approximately homogeneous (apart from small regions close to the fusion boundary). Furthermore, the weld metals are isotropic, i.e., they have the same mechanical (plasticity) response in all directions. This is not always the case in welds, which sometimes exhibit columnar zones in which there is pronounced texture. However, the samples studied were produced under standard (commercial) conditions, which are often designed to minimize both anisotropy and inhomogeneity, so this is not a surprising outcome. However, the parent plates did exhibit some anisotropy, with the through-thickness direction being slightly softer than the in-plane directions. The study of the radial symmetry of the indents provides a sensitive methodology for the detection of such anisotropy, and for obtaining an indication of its nature and strength, although the current PIP technology does not allow it to be fully characterized.

The PIP procedure has also been used to explore the mechanical properties in the transition regime between parent and weld. The outcome has been presented in the form of a plot of yield stress and (tensile) UTS against position. The spatial resolution

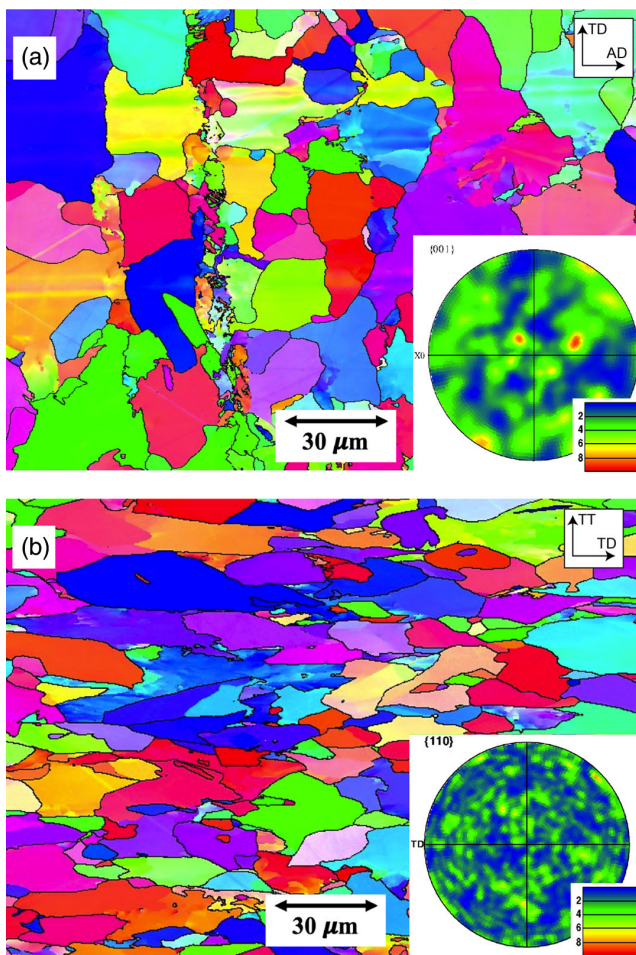


**Figure 9.** EBSD data, for the parent metal, showing grain structures and selected pole figures for a) an in-plane section and b) a transverse section.

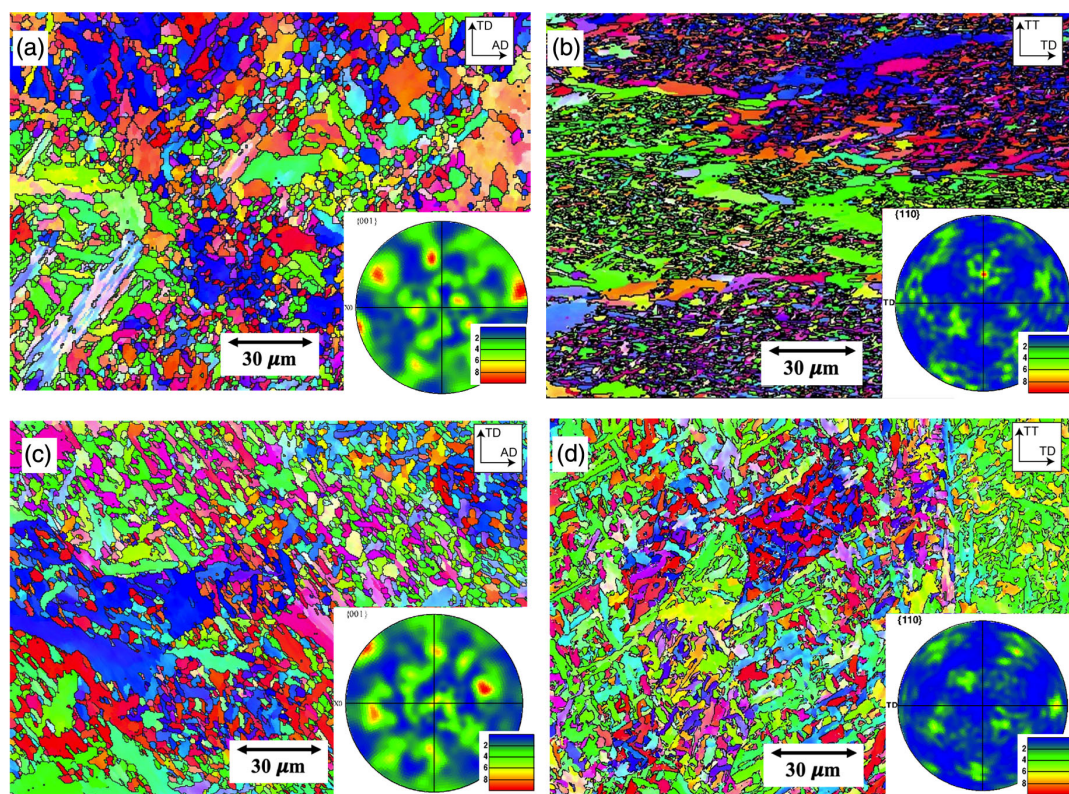


**Figure 10.** EBSD data showing grain structures and selected pole figures for a) an in-plane section of Weld 1, b) a transverse section of Weld 1, c) an in-plane section of Weld 2, and d) a transverse section of Weld 2.

of the technique is of the order of 1 mm. Some variations have been detected over distances of the order of several millimeters, attributed to parts of the parent close to the boundary having been significantly heated and parts of the weld close to the boundary having experienced higher cooling rates than the interior. Such information, which could be relevant to the mechanical performance of the weld under service conditions, cannot be obtained by conventional uniaxial testing (and is much more quantitative than the outcomes of hardness tests).

These results have been correlated to some extent with the outcomes of microstructural (EBSD) examination of both the weldments and the parent metal. These have confirmed that there is little or no systematic crystallographic texture in either the parent or the weldments. Moreover, there is no anisotropy in the grain structures of the welds, whereas there is some shape anisotropy in the parent, which could be responsible for the small amount of mechanical anisotropy exhibited by the parent (at high strain levels).

## Acknowledgements

This work was supported by the Bridging for Innovators Regional Centre Wales Programme, funded by BEIS, and the Science and Technology Facilities Council (STFC), via Grant No. ST/R006105/1. Financial support is also acknowledged from EPSRC, via Grant Nos. EP/M028267/1 and EP/I038691/1, and the European Social Fund (ESF) through the European Union's Convergence programme administered by the Welsh Government. Relevant support has also been received from

the Leverhulme Trust, in the form of an International Network grant (IN-2016-004) and an Emeritus Fellowship (EM/2019-038/4). The authors are also grateful to Alan Clark and Glenn Allen, both of TWI, for the provision of the welds and related information.

## Conflict of Interest

The authors declare no conflict of interest.

## Data Availability Statement

The data that support the findings of this study are available from the corresponding author upon reasonable request.

## Keywords

indentation plastometry, inverse finite element method (FEM), welds

Received: November 29, 2021

Revised: January 14, 2022

Published online: February 13, 2022

- [1] J. E. Campbell, H. Zhang, M. Burley, M. Gee, A. T. Fry, J. Dean, T. W. Clyne, *Adv. Eng. Mater.* **2021**, 23, 2001496.
- [2] Y. T. Tang, J. E. Campbell, M. Burley, J. Dean, R. C. Reed, T. W. Clyne, *Materialia* **2021**, 15, 101017.



- [3] M. Burley, J. E. Campbell, R. Reiff-Musgrove, J. Dean, T. W. Clyne, *Adv. Eng. Mater.* **2021**, 23, 2001478.
- [4] J. E. Campbell, M. Gaiser-Porter, W. Gu, S. Ooi, M. Burley, J. Dean, T. W. Clyne, *Adv. Eng. Mater.* **2021**, under review.
- [5] J. E. Campbell, T. Kalfhaus, R. Vassen, R. P. Thompson, J. Dean, T. W. Clyne, *Acta Mater.* **2018**, 154, 237.
- [6] T. W. Clyne, W. Gu, *Adv. Eng. Mater.* **2021**, 162, 2100739.
- [7] T. W. Clyne, J. E. Campbell, *Testing of the Plastic Deformation of Metals*, Cambridge University Press, Cambridge, UK **2021**.
- [8] S. Brandstetter, H. Van Swygenhoven, S. Van Petegem, B. Schmitt, R. Maass & P. M. Derlet, *Adv. Mater.* **2006**, 18, 1545.
- [9] B. Raeisinia, W. J. Poole, *Modell. Simul. Mater. Sci. Eng.* **2012**, 20, 015015.
- [10] G. D. Quinn, R. C. Bradt, *J. Am. Ceram. Soc.* **2007**, 90, 673.
- [11] T. W. Clyne, J. E. Campbell, M. Burley, J. Dean, *Adv. Eng. Mater.* **2021**, 23, 21004037.
- [12] F. M. Haggag, J. A. Wang, M. A. Sokolov, K. L. Murty, in *Symp. on Nontraditional Methods of Sensing Stress, Strain, and Damage in Materials and Structures*, Orlando, FL, **1996**, <https://doi.org/10.1520/stp11894s>.
- [13] T. S. Byun, J. H. Hong, F. M. Haggag, K. Farrell, E. H. Lee, *Int. J. Press. Vessels Pip.* **1997**, 74, 231.
- [14] I. M. Hutchings, *J. Mater. Res.* **2009**, 24, 581.
- [15] V. Bhasin, K. Sharma, P. K. Singh, K. K. Vaze, A. K. Ghosh, K. Madhusoodanan, B. B. Rupani, K. S. Balakrishnan, E. Ramadasan, S. Anantharaman, R. N. Singh, B. K. Gaur, V. Karthik, K. V. Kasiviswanathan, *Nucl. Eng. Des.* **2018**, 330, 303.
- [16] R. Pamnani, V. Karthik, T. Jayakumar, M. Vasudevan, T. Sakthivel, *Mater. Sci. Eng. A* **2016**, 651, 214.
- [17] S. Nagaraju, J. Ganesh Kumar, P. Vasantharaja, M. Vasudevan, K. Laha, *Mater. Sci. Eng. A* **2017**, 695, 199.
- [18] D. R. Barbadikar, T. Sakthivel, A. R. Ballal, D. R. Peshwe, R. S. Rao, M. D. Mathew, *Mater. High Temp.* **2018**, 35, 427.
- [19] J. Lee, K. Lee, S. Lee, O. M. Kwon, W. K. Kang, J. I. Lim, H. K. Lee, S. M. Kim, D. Kwon, *Materials* **2021**, 14, 2061.
- [20] S. Syngellakis, H. Habbab, B. G. Mellor, *Int. J. Comput. Methods Exp. Meas.* **2018**, 6, 527.
- [21] O. A. Katok, R. V. Kravchuk, V. V. Kharchenko, M. P. Rudnits'kyi, S. P. Bisyk, L. S. Davydovs'kyi, O. A. Slyvins'kyi, *Strength Mater.* **2020**, 52, 715.
- [22] G. Y. Sun, F. X. Xu, G. Y. Li, X. D. Huang, Q. Li, *Comput. Mater. Sci.* **2014**, 85, 347.
- [23] O. Iracheta, C. J. Bennett, W. Sun, *Int. J. Mech. Sci.* **2016**, 107, 253.
- [24] A. Evdokimov, A. Obrosof, R. Ossenbrink, S. Weiss, V. Michailov, *Mater. Sci. Eng. A*, **2018**, 722, 242.